

Article

Surface and Void Space Analysis of the Crystal Structures of Two Lithium Bis(pentafluoroethanesulfonyl)imide Salts

Anne Collart ¹ , Matthias Zeller ² and Patrick C. Hillesheim ^{1,3,*} 

¹ Department of Chemistry and Physics, Ave Maria University, Ave Maria, FL 34142, USA; anne.collart@my.avemaria.edu

² Department of Chemistry, Purdue University, West Lafayette, IN 47907, USA; zeller4@purdue.edu

³ Department of Chemistry and Physics, Florida Gulf Coast University, Fort Myers, FL 33965, USA

* Correspondence: patrick.hillesheim@avemaria.edu

Abstract: Analysis of two crystal structures of lithium bis(pentafluoroethanesulfonyl)imide is presented. Two orientations of the anion, that is a cis and trans orientation, are observed. Both structures exhibit unique interactions leading to the formation of discrete fluorine domains in the solid-state. A notable difference in the F...F interactions is seen when contrasting the two orientations wherein the trans geometry has a higher percentage of fluorine interactions than the cis orientation. The inclusion of water molecules in one of the structures also leads to the formation of a polar domain formed through a series of cyclical hydrogen bonding rings. The two structures allow for a detailed examination of the bond distances and angles involved in the formation of the two structures. Analysis of the void space in the two structures leads to the observation that the trans conformation exhibits notably higher void space as compared with the cis orientation. Hirshfeld surface analysis is used to help rationalize the interactions leading to unique changes in geometries and structure.



Citation: Collart, A.; Zeller, M.; Hillesheim, P.C. Surface and Void Space Analysis of the Crystal Structures of Two Lithium Bis(pentafluoroethanesulfonyl)imide Salts. *Crystals* **2022**, *12*, 701. <https://doi.org/10.3390/cryst12050701>

Academic Editor:
Waldemar Maniukiewicz

Received: 28 March 2022

Accepted: 11 May 2022

Published: 15 May 2022

Publisher's Note: MDPI stays neutral with regard to jurisdictional claims in published maps and institutional affiliations.



Copyright: © 2022 by the authors. Licensee MDPI, Basel, Switzerland. This article is an open access article distributed under the terms and conditions of the Creative Commons Attribution (CC BY) license (<https://creativecommons.org/licenses/by/4.0/>).

Keywords: crystal structure; alkali salts; surface analysis; ionic liquids

1. Introduction

An ionic liquid (IL) is a class of soft material that consists of a charge disperse organic cation and anion. It follows that the choice for which specific charge disperse anion to use is of vital importance for the rational design of ILs [1]. The field of ionic liquids has seen prolific development since the introduction of modern air and moisture stable anions [2,3]. The most common anions studied today typically contain fluorine groups which help disperse charges while also repelling other anions [4,5]. The three most common anions used in the synthesis of ILs are $[\text{PF}_6]^-$, $[\text{BF}_4]^-$, and $[\text{TF}_2\text{N}]^-$ [6]. ILs incorporating the tetrafluoroborate [2] and hexafluorophosphate [7] anions were reported first, followed by the introduction of the $[\text{TF}_2\text{N}]^-$ anion (see Figure 1) [8]. To date, the $[\text{TF}_2\text{N}]^-$ anion remains one of the most important anions given the favorable physicochemical properties it tends to impart on IL systems. However, other perfluoroalkyl-based anions capable of forming ILs have also been reported such as FAP [9], NCyF [10], and B(hfip)₄ (Figure 1) [11].

With approximately 1000 reported crystal structures [12], $[\text{TF}_2\text{N}]^-$ has found applications across a variety of fields. For example, $[\text{TF}_2\text{N}]^-$ has been used in catalyst design [13], in the formation of conductive materials [14], and in separations applications [15]. The crystal structures of the alkali salts of $[\text{TF}_2\text{N}]^-$ were reported by Xue et al. [16] In their studies, it was noted that the alkali salts have unique solvent behavior based on the nature of the alkali metal (i.e., Li vs. Rb). The inclusion of water and crystallization solvents was noted for several samples in the series examined. Further, it was found that the $[\text{TF}_2\text{N}]^-$ anion could exist in either the cis or trans isomers, simply defined by the orientation of the CF_3 groups with respect to the central S—N—S plane [17]. The trans isomer is energetically lower than the cis when examining the anion by itself [18]. In the presence of a metal ion, however, the anion often adopts the cis conformation to allow for the formation of

chelate rings from the sulfonyl oxygens. This appears to be the preferred orientation when interacting with metal cations, simply based on the reported structures in the CSD showing a preference for the cis isomer. It should be noted that there are reported examples wherein the trans conformation is seen binding to a metal also [19]. Both cis and trans conformations of $[\text{TF}_2\text{N}]^-$ have also been observed for several crystal structures of ILs [20,21]. The conformational flexibility of $[\text{TF}_2\text{N}]^-$ along with its charge dispersion and favorable thermal properties is what makes the anion particularly attractive for IL applications [1].

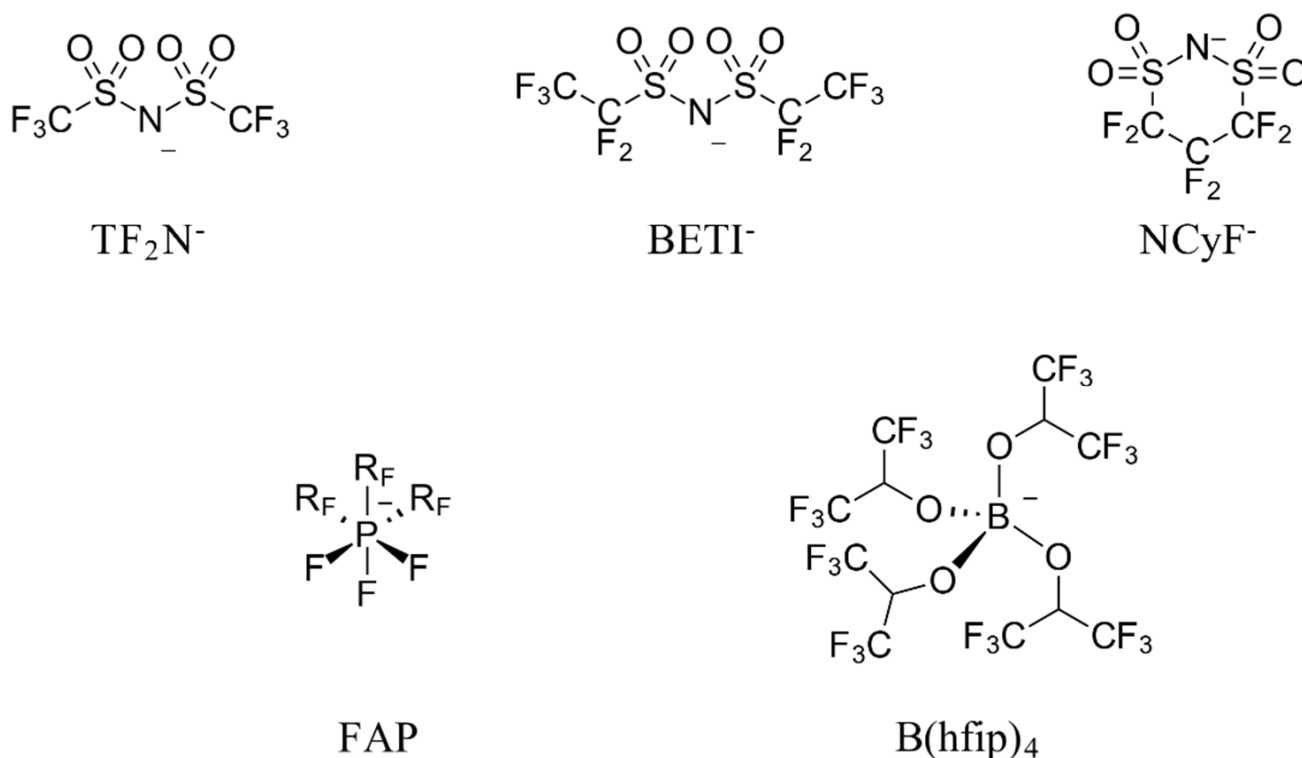


Figure 1. Common perfluorinated anions used in the development of ionic liquids and the abbreviations used herein.

In contrast to the many structures incorporating $[\text{TF}_2\text{N}]^-$, few $[\text{BETI}]^-$ structures that have been reported. Two reported structures are organometallic, with a cobaltocenium cation balancing the $[\text{BETI}]^-$ anion [22]. Three additional structures are classified into the realm of ILs given the use of quaternary ammonium cations [23–25]. A report by Henderson and Frech described the structures and thermal behavior of several glyme-coordinated $[\text{BETI}]^-$ species [26]. While structural reports on $[\text{BETI}]^-$ are limited, there are numerous reports detailing the use and application of $[\text{BETI}]^-$ anions, establishing this anion's diverse application across many fields of study. For example, $[\text{BETI}]^-$ has been used to form fluorescent materials [27]. Further, $[\text{BETI}]^-$ has been used for carbon capture systems, helping to improve solubility when compared with other structurally related perfluorinated anions in the study [28]. Systems incorporating the $[\text{BETI}]^-$ anion have also been applied for extractions, specifically in the separation of rare-earth metals [29].

As expected, based on the structural and compositional similarities, $[\text{BETI}]^-$ shares several parallels with $[\text{TF}_2\text{N}]^-$. For example, both anions impart high thermal stability for ILs while simultaneously depressing the melting point [30]. Structurally, the $[\text{BETI}]^-$ anion can adopt both a cis or trans conformation as well [23]. The energetics of the conformers were examined by the Davis group and found that similar to $[\text{TF}_2\text{N}]^-$, there is an energetic preference for the trans conformation [31]. Given the increased ethyl chain length it is also likely that there would exist additional conformers arising from unique rotations of the ethyl chains in combination with the cis/trans isomers. A more in-depth computational and

experimental investigation of $[\text{BETI}]^-$ would certainly be of benefit to the IL community, especially in light of the anion crisis [32].

Herein we present the crystal structure of lithium bis(pentafluoroethanesulfonyl)imide and diaqua lithium bis(pentafluoroethanesulfonyl)imide. Given that the lithium salts are fundamental components in the synthesis of ILs, and that the metathesis of ILs is typically carried out in an aqueous solution, understanding the structure of the alkali salts of $[\text{BETI}]^-$ is of importance to the broader scientific community. Further, these two crystal structures represent some of the few current examples of simple metal complexes with this anion. The high-resolution structures are also of importance for the development of theoretical models to understand the electronic structure of the anion allowing for the development of novel materials [33]. Moreover, the $[\text{BETI}]^-$ anion is observed in a cis and trans orientations, allowing for a more in-depth analysis of variations brought about by these unique conformers.

2. Materials and Methods

2.1. Chemicals

Lithium bis(pentafluoroethanesulfonyl)imide was purchased from TCI Chemicals and used as is without further purification.

2.2. Single Crystal Diffraction

Single crystals suitable for X-ray diffraction were grown from a saturated aqueous solution of the anhydrous LiBETI salt. The solution was placed in a 10 mL scintillation vial and loosely capped to allow for evaporation. Slow evaporation over 10 months yielded both sets of crystals in a single vial.

Single crystals of both samples were coated with a trace of Fomblin oil and were transferred to the goniometer head of a Bruker Quest diffractometer. Data collection of $[\text{Li}\{\text{BETI}\}]$ used Cu $K\alpha$ wavelength ($\lambda = 1.54178 \text{ \AA}$) on an instrument with kappa geometry, an I- μ -S microsource X-ray tube, laterally graded multilayer (Goebel) mirror single crystal for monochromatization, and a PhotonIII_C14 area detector while $[\text{Li}\{\text{BETI}\}(\text{H}_2\text{O})_2]$ was collected using Mo $K\alpha$ wavelength ($\lambda = 0.71073 \text{ \AA}$) on an instrument with a fixed chi angle, a sealed tube fine focus X-ray tube, single crystal curved graphite incident beam monochromator and a PhotonII area detector. Both instruments are equipped with an Oxford Cryosystems low temperature device and examination and data collection were performed at 150 K. Data were collected, reflections were indexed and processed, and the files scaled and corrected for absorption using APEX3 [34] and SADABS [35]. The space groups were assigned and the structures were solved by direct methods using XPREP within the SHELXTL [36] suite of programs and refined by full matrix least squares against F^2 with all reflections using Shelxl2018 [37] and the graphical interfaces Shelxle [38] and Olex2 [39]. Water H atoms were located as electron density and were refined. O-H bond distances were restrained to $0.84(2) \text{ \AA}$. $U_{\text{iso}}(\text{H})$ values were set to a 1.5 times $U_{\text{eq}}(\text{O})$.

Complete crystallographic data, in CIF format, have been deposited with the Cambridge Crystallographic Data Centre. Table 1 contains the relevant crystallographic data for both compounds. CCDC 2126084 and 2126085 contains the supplementary crystallographic data for this paper. These data can be obtained free of charge from The Cambridge Crystallographic Data Centre via www.ccdc.cam.ac.uk/data_request/cif.

Table 1. Crystallographic data and refinement details for [Li{BETI}] and Li{BETI}(H₂O)₂.

	Li{BETI}	Li{BETI}(H ₂ O) ₂
Chemical formula	C ₄ F ₁₀ LiNO ₄ S ₂	C ₄ H ₄ F ₁₀ LiNO ₆ S ₂
<i>M_r</i>	387.11	423.14
Crystal system, space group	Monoclinic, C2/c	Triclinic, <i>P</i> $\bar{1}$
Temperature (K)	150	150
<i>a</i> , <i>b</i> , <i>c</i> (Å)	42.733 (5), 5.4927 (7), 10.4751 (14)	6.4581 (3), 8.0725 (4), 13.0495 (5)
α (°)	90	95.160 (3)
β (°)	99.632 (11)	103.406 (3)
γ (°)	90	91.403 (3)
<i>V</i> (Å ³)	2424.0 (5)	658.37 (5)
<i>Z</i>	8	2
Radiation type	Cu <i>K</i> α	Mo <i>K</i> α
μ (mm ⁻¹)	5.50	0.56
Crystal size (mm)	0.21 × 0.15 × 0.02	0.20 × 0.05 × 0.03
Data collection		
Diffractometer	Bruker AXS D8 Quest diffractometer with PhotonIII_C14 charge-integrating and photon counting pixel array detector	Bruker AXS D8 Quest diffractometer with PhotonII charge-integrating pixel array detector (CPAD)
Absorption correction	Multi-scan SADABS 2016/2	Multi-scan SADABS 2016/2
<i>T</i> _{min} , <i>T</i> _{max}	0.503, 0.754	0.676, 0.747
No. of measured, independent and observed [<i>I</i> > 2σ(<i>I</i>)] reflections	7332, 2443, 1991	21544, 4985, 3337
<i>R</i> _{int}	0.097	0.066
(sin θ /λ) _{max} (Å ⁻¹)	0.638	0.770
Refinement		
<i>R</i> [<i>F</i> ² > 2σ(<i>F</i> ²)], <i>wR</i> (<i>F</i> ²), <i>S</i>	0.042, 0.112, 1.05	0.042, 0.091, 1.01
No. of reflections	2443	4985
No. of parameters	199	229
$\Delta\rho_{\max}$, $\Delta\rho_{\min}$ (e Å ⁻³)	0.36, -0.38	0.49, -0.54

2.3. Software

Hirshfeld surfaces, images, and fingerprint plots were calculated and produced using CrystalExplorer17 [40]. Discussion about the analysis of fingerprints and surfaces can be found in the appropriate references [41,42]. Images and analysis of the structures was accomplished using Olex2 [39]. Void space images and calculations were accomplished using Mercury [43]. Void spaces were calculated with a 0.8 Å probe radius.

3. Results and Discussion

[Li{BETI}] crystallizes in the C2/c space group with one molecule in the asymmetric unit. [Li{BETI}(H₂O)₂] crystallizes in the *P* $\bar{1}$ space group, also with one molecule in the asymmetric unit. The asymmetric units of both structures are shown in Figure 2. In both structures, the sulfonyl oxygen atoms are binding to the metal center forming a six-membered chelate ring. Despite forming a similar chelate structure, there are several notable differences in the structures. For example, in [Li{BETI}], the sulfonyl groups

make shorter bonds to the lithium with S—O⋯Li distances of 1.927(5) and 1.917(5). In [Li{BETI}(H₂O)₂], however, the distances are slightly longer with S—O⋯Li distances of 2.094(4) and 2.163(3). One noteworthy distinction between [Li{BETI}] and [Li{BETI}(H₂O)₂] is that [Li{BETI}(H₂O)₂] is the first example of the [BETI][−] anion in the cis geometry wherein the anion is not disordered [23]. As discussed above, the [TF₂N][−] anion exists both in the cis and trans geometry, with there appearing to be an approximately equal distribution of both isomers in the reported crystalline structures. Currently, however, [Li{BETI}] has only been reported in the lower energy trans conformation.

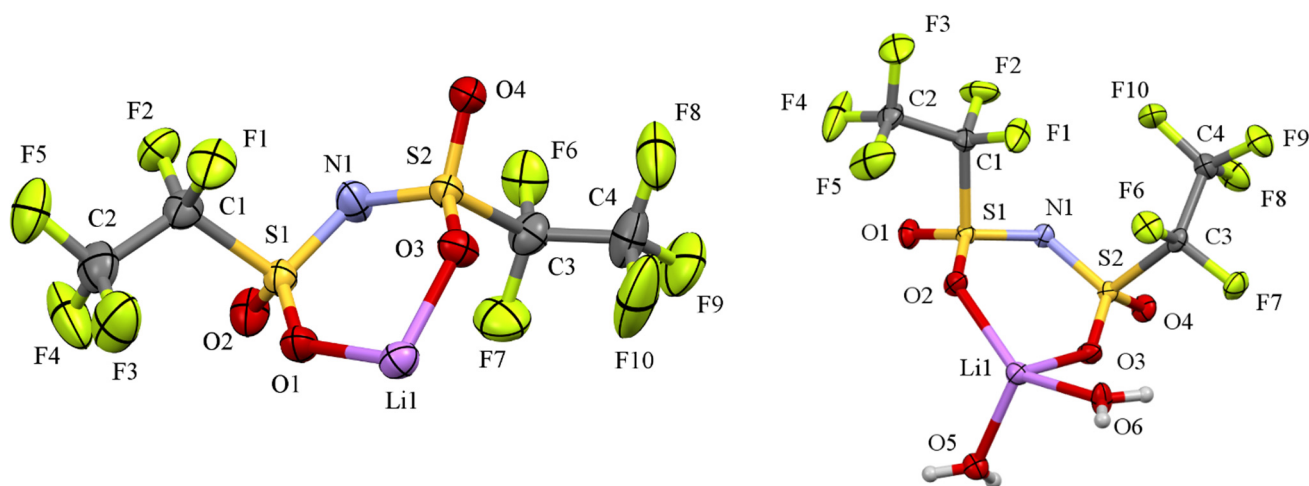


Figure 2. Asymmetric units of [Li{BETI}] (**left**) and [Li{BETI}(H₂O)₂] (**right**) shown with 50% probability ellipsoids. Gray, carbon; green, fluorine; red, oxygen; pink, lithium; yellow, sulfur; blue, nitrogen.

Several potential factors influence the distances and interactions in the two molecules. Predominantly, the coordination geometry of the lithium is a factor. In [Li{BETI}], the lithium exists in a pseudo-tetrahedral geometry with four oxygen atoms making bonds to the metal. Two of the oxygens are from a single bidentate [BETI][−] anion, and the remaining oxygens are from symmetry adjacent anions, effectively making an infinite chain linked through the lithium ion (see Figure 3). In [Li{BETI}(H₂O)₂], the lithium atom exists in a distorted trigonal bipyramidal geometry with two water molecules, one bidentate [BETI][−] anion, and a single sulfonyl oxygen from an adjacent anion making up the coordination sphere (see Figure 3). The hydrated structure, thus, forms a near-linear arrangement of the lithium ions. The bound water molecules help arrange the layers of the structure by forming reciprocal hydrogen bonds to symmetry adjacent water molecules. The unique coordination in addition to the cis/trans geometries lead to distinctive arrangements of the structures.

The long-range ordering of both structures does share similarities, as expected (see Figure 4). For instance, both show distinctive fluorine layers wherein the perfluoroalkyl groups are in close contact with each other. Further, there exists a distinct layer wherein the lithium ions and sulfonyl groups exist. The inclusion of the serendipitous water molecules in [Li{BETI}(H₂O)₂], in addition to the structural changes associated with the coordination of the lithium ion, influences the void space in the lattice (see Figure 5). Examining Figure 5 one can readily observe the differences in the two structures. [Li{BETI}] has significantly higher void space in the lattice (5.8% of volume, 140.59 Å³) as compared with [Li{BETI}(H₂O)₂] (1.1% of volume, 7.03 Å³). [Li{BETI}] has void space near the lithium ion as well as in the fluorine domain whereas the voids in [Li{BETI}(H₂O)₂] are in the hydrophilic pocket formed by the waters and sulfonyl oxygen atoms. The differences in the void space is also observed through examining the varied interactions in the crystalline structures (*vide infra*).

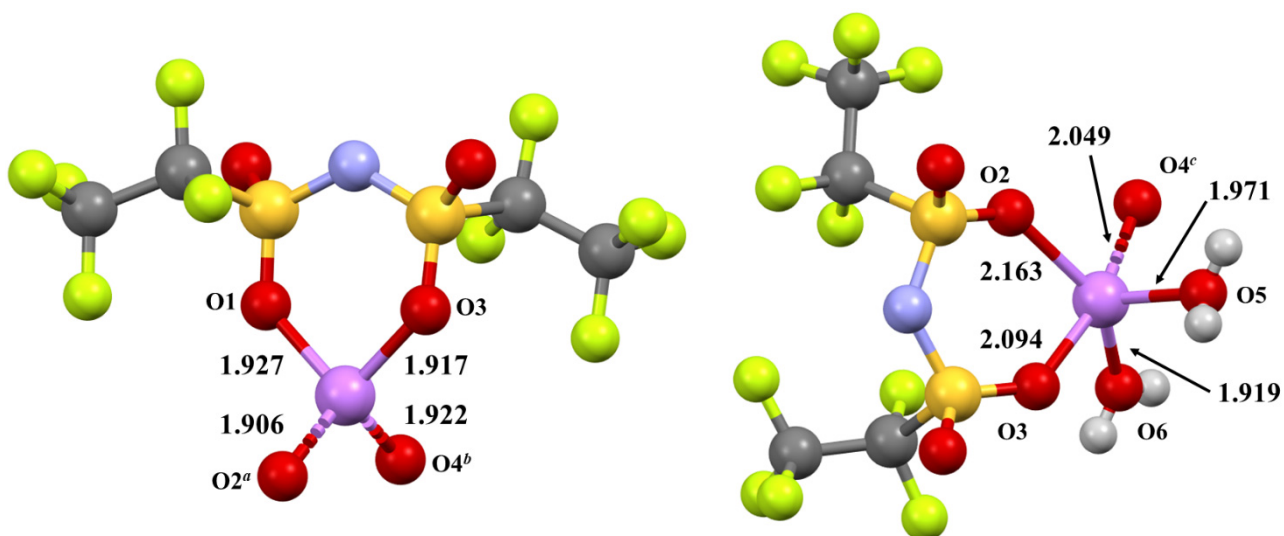


Figure 3. Images depicting the lithium cation coordination geometry for [Li{BETI}] (left) and [Li{BETI}(H₂O)₂] (right). Bond distances are shown in Å. Dashed bonds indicate symmetry adjacent atoms. $a = +x, -y, \frac{1}{2} + z$; $b = +x, -1 + y, +z$; $c = -1 + x, +y, +z$.

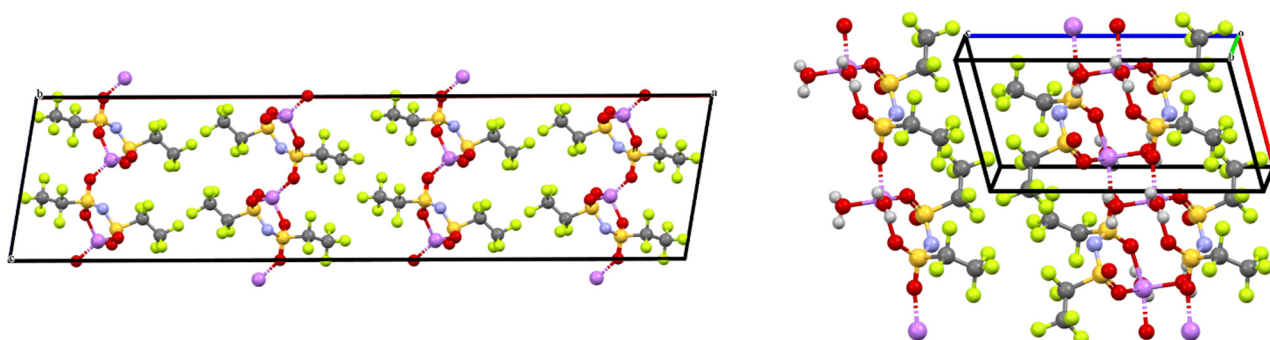


Figure 4. Packing diagrams for [Li{BETI}] (left) and [Li{BETI}(H₂O)₂] (right). Alternating layers of fluorine and oxygen atoms are prominent features of both structures. Unit cells are shown for references.

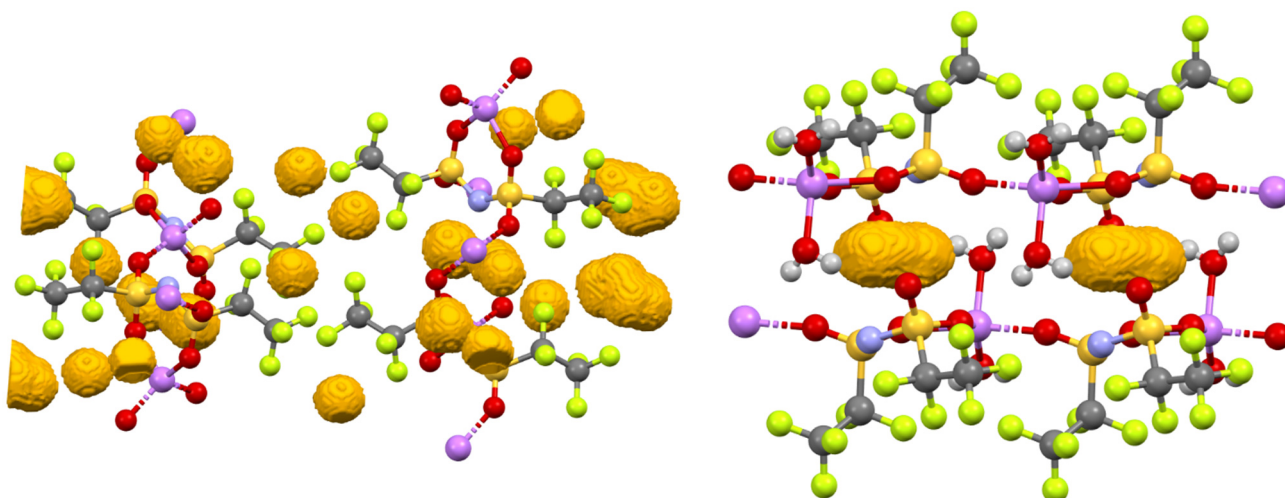


Figure 5. Visualization of the void space (yellow spheres) in [Li{BETI}] (left) and [Li{BETI}(H₂O)₂] (right).

To better understand the interactions and structures of the two compounds, Hirshfeld surface analysis was performed [44]. The surfaces for both structures are shown in Figures 6 and 7, respectively, and the fingerprint plots [41] in Figure 8. Several key similarities are observed in the fingerprints of the structures. A diagonal region of red interactions is observed in both fingerprints, indicative of a large number of interactions at similar distances [45]. These interactions are primarily from F...F interactions. Further, there are regions of disperse spots in both fingerprints, especially at longer distances ($d_i \approx d_e \approx 2.5 \text{ \AA}$). These disperse spots can be indicative of inefficient crystal packing. While not directly quantifiable, the increased void space in [Li{BETI}] is observed as the larger regions of disperse interactions seen in the fingerprint for [Li{BETI}] when contrasted with [Li{BETI}(H₂O)₂]. Finally, a set of pincer-like features are seen in both structures, with [Li{BETI}] showing more pronounced features. These shapes arise from the fact that the structures are polymeric, forming interactions linking multiple asymmetric units through O...Li bonds which form the pincer shapes. These bonds manifest as the indicated red indentations observed on the d_{norm} surfaces (Figures 6 and 7).

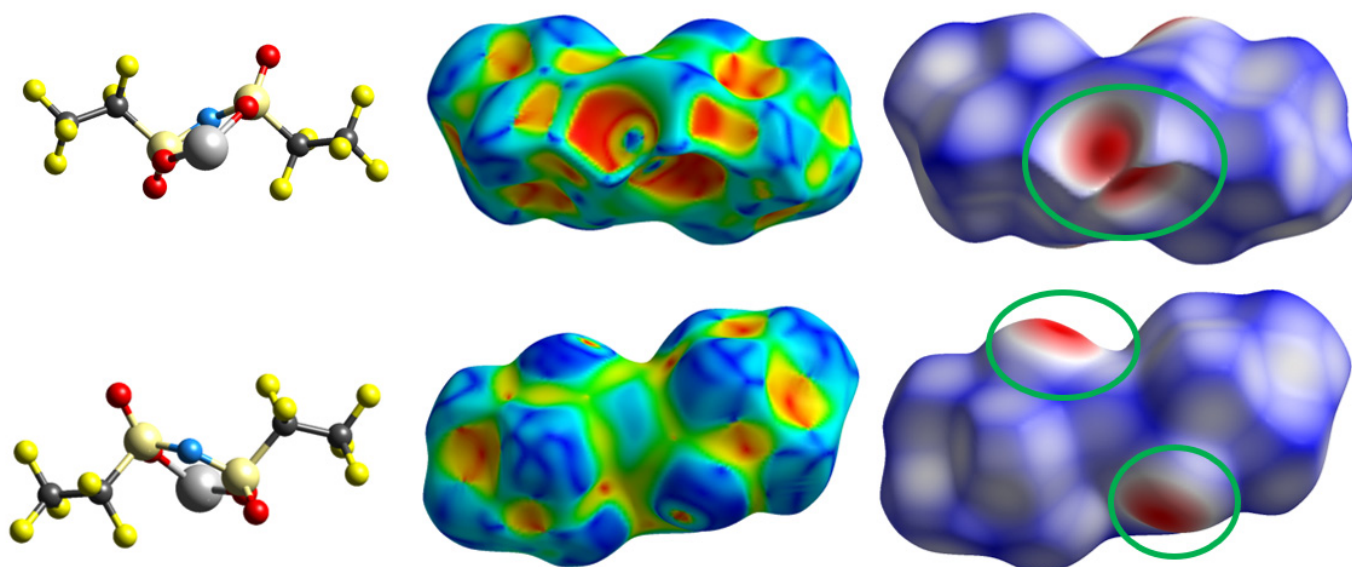


Figure 6. Depiction of the [Li{BETI}] structure (left) and the Hirshfeld surfaces for [Li{BETI}] mapped with the shape index (middle) and d_{norm} (right). Green circles indicate the connection points for the oxygen atoms to adjacent lithium ions.

Several key differences can also be observed when looking at the fingerprints (Figure 8). Looking at the shape of the fingerprints at higher d_i/d_e values, [Li{BETI}] shows a flared tail while [Li{BETI}(H₂O)₂] tapers to a blunted end. As discussed, this corroborates the void space analysis and the differences between the two structures. Looking closely at the F...F interactions in both fingerprints (the diagonal red line, *vide supra*), [Li{BETI}(H₂O)₂] displays shorter interactions as observed by the starting distances of the red line in [Li{BETI}(H₂O)₂] ($d_i \approx d_e \approx 1.5 \text{ \AA}$) vs. [Li{BETI}] ($d_i \approx d_e \approx 1.7 \text{ \AA}$). Additionally, the shape of this red region is unique between the two molecules with [Li{BETI}(H₂O)₂] having a more distinct, narrow red line while the interactions in **1** manifest as a more disperse set. This observation points to the unique sets of interactions that are present in both structures.

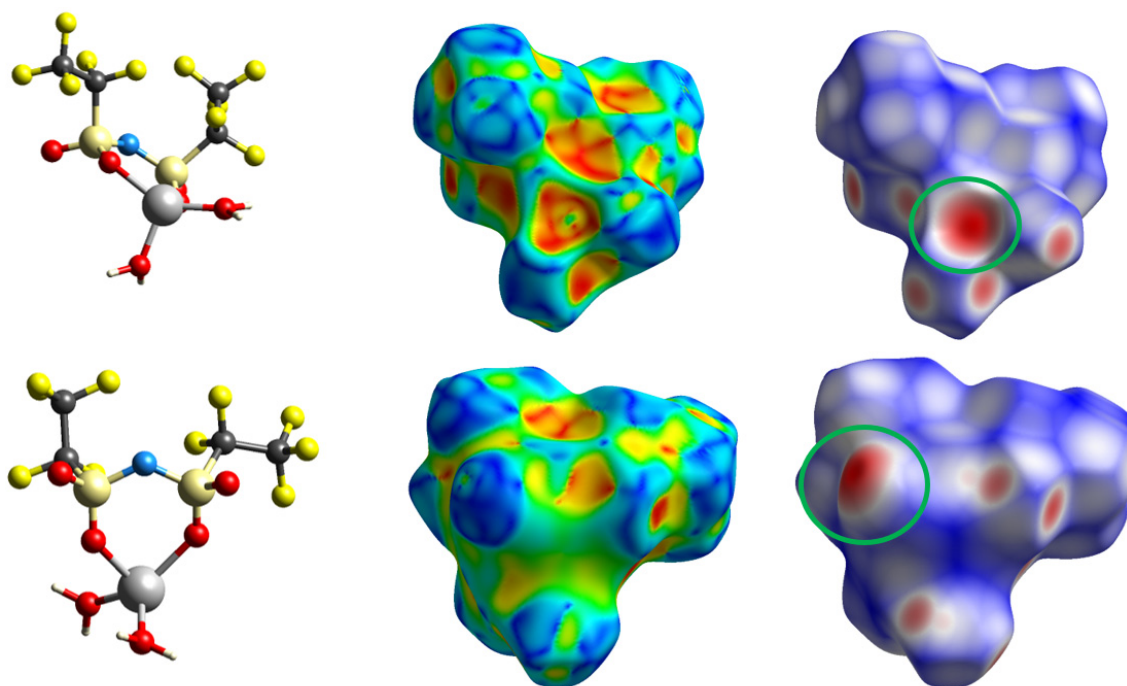


Figure 7. Depiction of the $[\text{Li}\{\text{BETI}\}(\text{H}_2\text{O})_2]$ structure (left) and the Hirshfeld surfaces for $[\text{Li}\{\text{BETI}\}(\text{H}_2\text{O})_2]$ mapped with the shape index (middle) and d_{norm} (right). Green circles indicate the points wherein the oxygen atoms coordinate to the lithium ions in adjacent molecules.

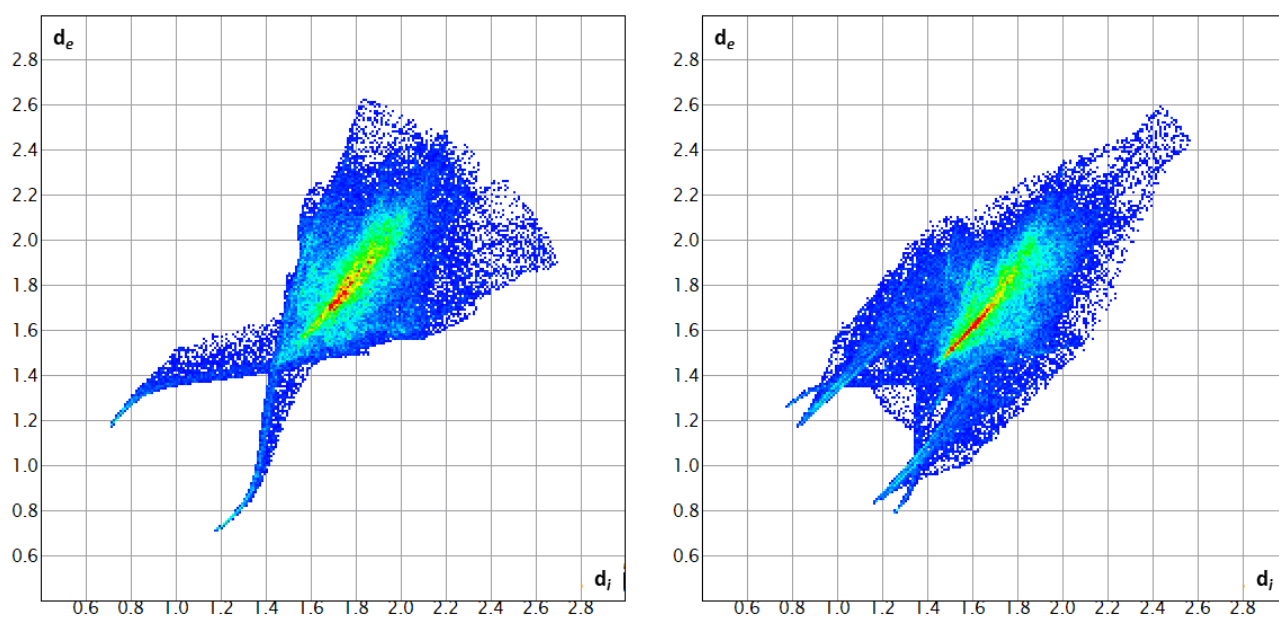


Figure 8. The fingerprint plots for $[\text{Li}\{\text{BETI}\}]$ (left) and $[\text{Li}\{\text{BETI}\}(\text{H}_2\text{O})_2]$ (right).

The total percentage of $\text{F}\cdots\text{F}$ interactions is higher in $[\text{Li}\{\text{BETI}\}]$ (60.5%) than in $[\text{Li}\{\text{BETI}\}(\text{H}_2\text{O})_2]$ (46.3%). This may seem to suggest that the $\text{F}\cdots\text{F}$ interactions are, in some way, favorable. However, this change in percentage is simply due to the positioning of the perfluoroethyl chain in $[\text{Li}\{\text{BETI}\}(\text{H}_2\text{O})_2]$. The cis orientation places atoms F1, F6, F10 in close proximity intramolecularly, effectively preventing any intermolecular interactions from these three positions. The trans structure, however, does not show any steric ‘blocking’ of fluorine atoms, leading to an increased percentage of $\text{F}\cdots\text{F}$ interactions overall. Further, there are no $\text{O}\cdots\text{H}\cdots\text{F}$ interactions observed arising from the water molecules in $[\text{Li}\{\text{BETI}\}(\text{H}_2\text{O})_2]$, implying that the change in $\text{F}\cdots\text{F}$ interactions is not influenced by the

presence of water and the potential hydrogen bonding. It should be stated that reports have shown F...F interactions to be destabilizing or, at the least, do not stabilize packing [46] though some reports seem to contradict this [47].

Given the packing of the anions into discrete fluorine domains, along with the results of the surface analysis, we sought for evidence of any F...F halogen bonds [48–50]. While the existence of halogen bonding between fluorine atoms remains debated [51], there are a number of shorter contacts between fluorine atoms which may be evidence of type II halogen bonding. For example, the terminal CF₃ group in [Li{BETI}] shows close contacts with a symmetry adjacent CF₃ group ($i = 1 - x, -y, 1 - z$). Specifically, F4 is interacting with F4ⁱ at a distance of 3.045(6) Å ($\angle C2-F4...F4^i = 93.3(3)^\circ$). F6 also exhibits F...F interactions at similar distances to those seen with F4 ($d(F6...F8^j) = 3.087(4)$ Å, $\angle C3-F6...F8^j = 126.6(2)$, $j = x, 1 - y, -1/2 + z$). These close interactions are seen on the shape index surface as the indicated red/yellow indentations (see Figures 6 and 7). Aside from these interactions, however, we do not observe any defined halogen bonding. For clarity, the F...F interactions for both molecules are visualized in Figure 9, allow for comparison between the two structures.

Table 2 shows a complete listing of the total interaction percentages arising from specific elements in both structures. As expected, the fluorine atoms dominate the intermolecular interactions (by percentage) followed by the oxygen. The roles of the oxygen interactions are unique, however, when contrasting structures 1 and 2. Given the presence of the water molecules in 2, hydrogen bonding is observed, linking discrete asymmetric units together. A depiction of a portion of the hydrogen bonding is shown in Figure 10. Further, the hydrogen bonding is observed as the reciprocal set of spikes in the fingerprint plot ($d_i \approx 1.1$ Å, $d_e \approx 0.9$ Å) and at the appropriate reciprocal distances, that is $d_i \approx 0.9$ Å, $d_e \approx 1.1$ Å. Overall the hydrogen bonding in [Li{BETI}(H₂O)₂] is quite complex, with several unique set of hydrogen bonding rings being observed [52]. Two $R_2^2(8)$ rings are formed from the reciprocal interactions between O2 and O5 and O5 and O6. These are highlighted as green and yellow, respectively, in Figure 9. With respect to the O2 and O5 hydrogen interactions, the distance is 2.32 Å ($d(O2...H5B^m, m = -x, 1 - y, 1 - z)$). The O5 and O6 hydrogen interactions distance is 2.22 Å ($d(O5...H6B^n, n = -x, 2 - y, 1 - z)$). An additional $R_3^3(8)$ ring is observed involving the two water molecules (O5 and O6) and two sulfonyl oxygens O1 and O2. This is shown as the purple highlighted ring in Figure 9. The distances between O5 and O2 as well as O5 and O6 are given previously, 2.32 Å and 2.22 Å, respectively. The O1...H6A distance is 2.16 Å ($d(O1...H6A^o, o = +x, 1 + y, +z)$). The arrangement of these rings and formation of the hydrogen bonding network help to form the void space discussed within the structure of [Li{BETI}(H₂O)₂].

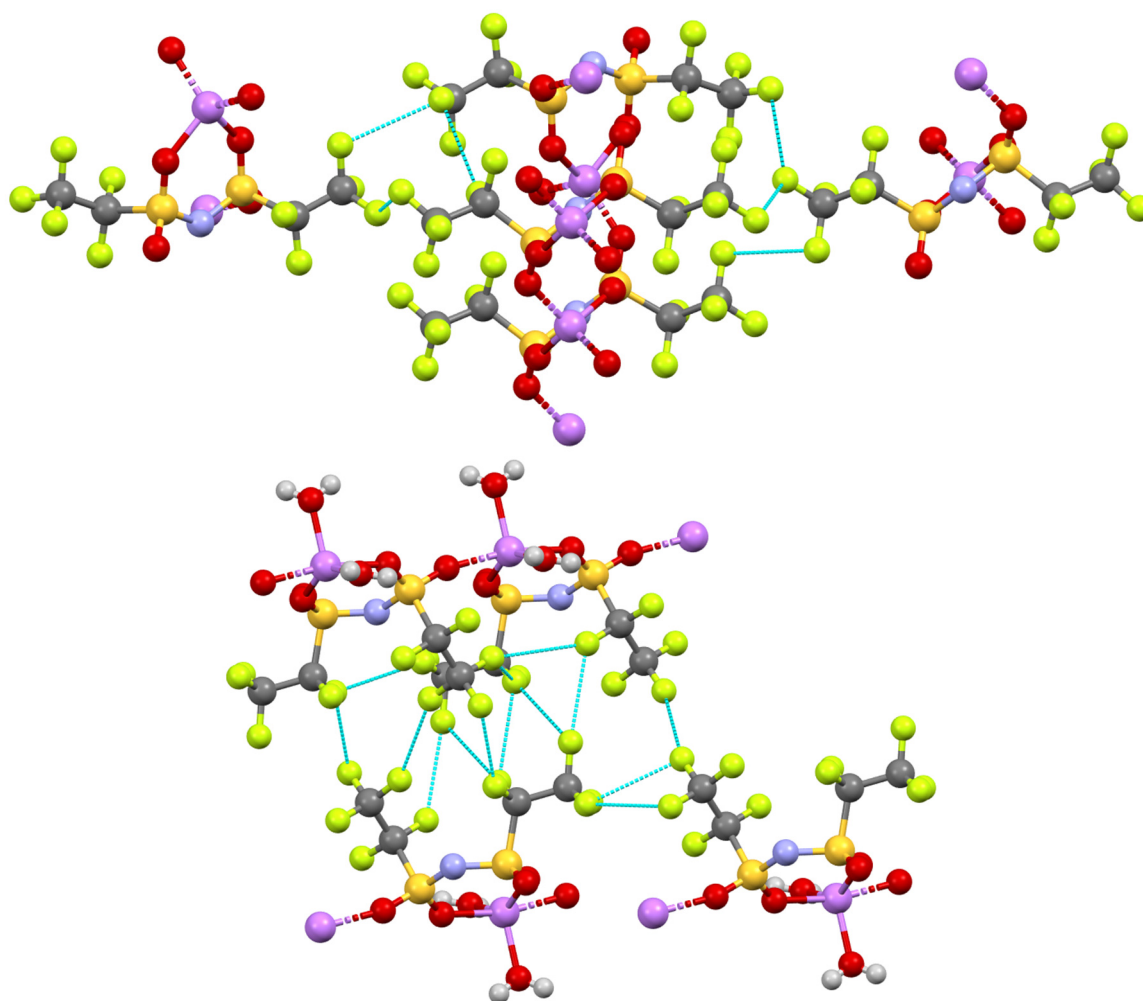


Figure 9. Depiction of the F...F interactions (light blue lines) in [Li{BETI}] (**top**) and [Li{BETI}(H₂O)₂] (**bottom**).

Table 2. Calculated interactions of atoms in both [Li{BETI}] and [Li{BETI}(H₂O)₂] based on Hirshfeld surface calculations.

	[Li{BETI}]	[Li{BETI}(H ₂ O) ₂]
F...All	69.5%	54.9%
O...All	19.9%	21.2%
N...All	2.5%	2.4%

Given the absence of water molecules, the oxygen atoms in **1** show a markedly different set of interactions. Predominantly there are no overtly stabilizing non-covalent interactions [53,54] arising from the oxygen atoms. All four of the oxygen atoms are binding to a lithium ion, with O1 and O3 acting as the bidentate binding points, while O2 and O4 act as the bridging points to the adjacent lithium ions. The majority of the ~20% of the O interactions in [Li{BETI}] arise from long-distance O...F interactions. The distances and angles examined do not seem to indicate any form of chalcogen bonds being formed [55]. Additional interactions between O and N and O and O complete the noteworthy interactions observed in [Li{BETI}]. From our perspective, neither the O...N nor O...O interactions are stabilizing but are simply an artifact of the packing from the crystal based on the distances and angles observed.

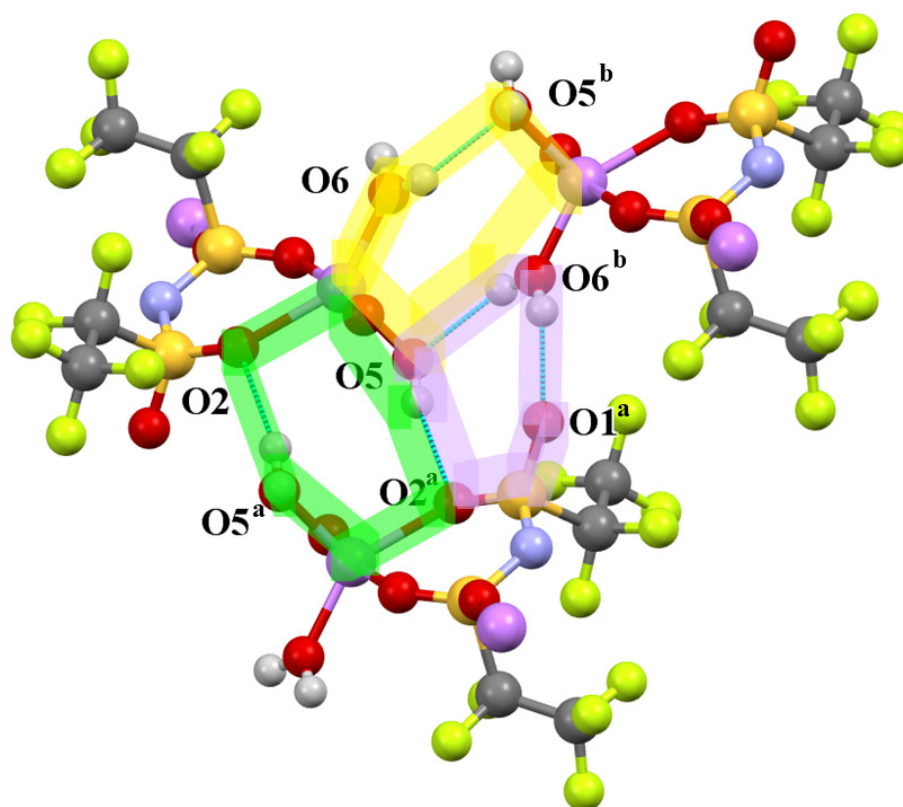


Figure 10. Depiction of hydrogen bonding ring interactions in $[\text{Li}\{\text{BETI}\}(\text{H}_2\text{O})_2]$. Different highlights are used to distinguish different hydrogen bonding rings which are formed. Green = $R_2^2(8)$; purple $R_3^3(8)$; yellow = $R_2^2(8)$. a = $-x, 1 - y, 1 - z$; b = $-x, 2 - y, 1 - z$.

4. Conclusions

The two crystal structures of lithium bis(pentafluoroethanesulfonyl)imide and lithium bis(pentafluoroethanesulfonyl)imide diaqua are reported. These structures represent two new samples for the sparse but growing set of structural data for the $[\text{BETI}]^-$ anion. The two structures clearly show the cis and trans geometries of the anion, allowing for the detailed examination of distances and angles arising from this change in structure. For example, the cis geometry displays unique intramolecular $\text{F}\cdots\text{F}$ interactions due to the proximity of the perfluoroalkyl chains. Thus, the diaqua structure shows a lower $\text{F}\cdots\text{F}$ interaction percentage due to the arrangements of the perfluoroethyl chains hindering intermolecular interactions. In contrast, the trans geometry allows for increased interactions with the perfluoroalkyl chains. Overall, $\text{F}\cdots\text{F}$ close-contacts making up the majority of the interactions present in the solid-state.

$[\text{Li}\{\text{BETI}\}(\text{H}_2\text{O})_2]$, however, shows significantly lower void space in the crystal structure due, in part, to shorter $\text{F}\cdots\text{F}$ interactions and hydrogen bonding arising from the water molecules. The hydrogen bonding in the molecule is quite unique, with three distinctive reciprocal hydrogen bonding rings formed. Given the linear nature of hydrogen bonds, a void pocket is formed within the region wherein the bound water molecules are located.

Author Contributions: A.C.: writing—original draft, review and editing, formal analysis; M.Z.: data curation, investigation, writing—review and editing, formal analysis; P.C.H.: conceptualization, methodology, validation, visualization, formal analysis, supervision, project administration, writing—original draft, review and editing. All authors have read and agreed to the published version of the manuscript.

Funding: Parts of this material is based upon work supported by the National Science Foundation through the Major Research Instrumentation Program under Grants No. CHE-1625543. The APC was funded by Ave Maria University Department of Chemistry and Physics.

Institutional Review Board Statement: Not applicable.

Informed Consent Statement: Not applicable.

Data Availability Statement: Not applicable.

Acknowledgments: This work was supported by Ave Maria University Department of Chemistry and Physics and Florida Gulf Coast University Department of Chemistry and Physics.

Conflicts of Interest: The authors declare no conflict of interest.

References

1. MacFarlane, D.R.; Kar, M.; Pringle, J.M. *Fundamentals of Ionic Liquids*; Wiley-VCH Verlag GmbH & Co. KGaA: Weinheim, Germany, 2017. [[CrossRef](#)]
2. Wilkes, J.S.; Zaworotko, M.J. Air and Water Stable 1-Ethyl-3-Methylimidazolium Based Ionic Liquids. *J. Chem. Soc. Chem. Commun.* **1992**, *13*, 965–967. [[CrossRef](#)]
3. Deetlefs, M.; Farnsworth, M.; Seddon, K.R. Ionic Liquids: The View from Mount Improbable. *RSC Adv.* **2016**, *6*, 4280–4288. [[CrossRef](#)]
4. Dupont, J. On the Solid, Liquid and Solution Structural Organization of Imidazolium Ionic Liquids. *J. Braz. Chem. Soc.* **2004**, *15*, 341–350. [[CrossRef](#)]
5. Wang, Y.; Parvis, F.; Hossain, I.; Ma, K.; Jarošová, R.; Swain, G.M.; Blanchard, G.J. Local and Long-Range Organization in Room Temperature Ionic Liquids. *Langmuir* **2021**, *37*, 605–615. [[CrossRef](#)] [[PubMed](#)]
6. Welton, T. Ionic Liquids: A Brief History. *Biophys. Rev.* **2018**, *10*, 691–706. [[CrossRef](#)] [[PubMed](#)]
7. Fuller, J.; Carlin, R.T.; De Long, H.C.; Haworth, D. Structure of 1-Ethyl-3-Methylimidazolium Hexafluorophosphate: Model for Room Temperature Molten Salts. *J. Chem. Soc. Chem. Commun.* **1994**, *3*, 299. [[CrossRef](#)]
8. Bonhôte, P.; Dias, A.-P.; Papageorgiou, N.; Kalyanasundaram, K.; Grätzel, M. Hydrophobic, Highly Conductive Ambient-Temperature Molten Salts. *Inorg. Chem.* **1996**, *35*, 1168–1178. [[CrossRef](#)] [[PubMed](#)]
9. Ignat'ev, N.V.; Welz-Biermann, U.; Kucheryna, A.; Bissky, G.; Willner, H. New Ionic Liquids with Tris(Perfluoroalkyl)Trifluorophosphate (FAP) Anions. *J. Fluor. Chem.* **2005**, *126*, 1150–1159. [[CrossRef](#)]
10. Philippi, F.; Welton, T. Targeted Modifications in Ionic Liquids—from Understanding to Design. *Phys. Chem. Chem. Phys.* **2021**, *23*, 6993–7021. [[CrossRef](#)]
11. Kaliner, M.; Rupp, A.; Krossing, I.; Strassner, T. Tunable Aryl Alkyl Ionic Liquids with Weakly Coordinating Tetrakis((1,1,1,3,3,3-Hexafluoropropan-2-yl)Oxy)Borate [B(Hfip)₄] Anions. *Chem.–Eur. J.* **2016**, *22*, 10044–10049. [[CrossRef](#)]
12. Groom, C.R.; Bruno, I.J.; Lightfoot, M.P.; Ward, S.C. The Cambridge Structural Database. *Acta Crystallogr. Sect. B Struct. Sci. Cryst. Eng. Mater.* **2016**, *72*, 171–179. [[CrossRef](#)] [[PubMed](#)]
13. Hashmi, A.S.K.; Braun, I.; Rudolph, M.; Rominger, F. The Role of Gold Acetylides as a Selectivity Trigger and the Importance of Gem-Diaurated Species in the Gold-Catalyzed Hydroarylation-Aromatization of Arene-Dienes. *Organometallics* **2012**, *31*, 644–661. [[CrossRef](#)]
14. Cheng, Y.; Yang, J.; Hung, J.-H.; Patra, T.K.; Simmons, D.S. Design Rules for Highly Conductive Polymeric Ionic Liquids from Molecular Dynamics Simulations. *Macromolecules* **2018**, *51*, 6630–6644. [[CrossRef](#)]
15. Fan, F.-L.; Qin, Z.; Cao, S.-W.; Tan, C.-M.; Huang, Q.-G.; Chen, D.-S.; Wang, J.-R.; Yin, X.-J.; Xu, C.; Feng, X.-G. Highly Efficient and Selective Dissolution Separation of Fission Products by an Ionic Liquid [Hbet][Tf₂N]: A New Approach to Spent Nuclear Fuel Recycling. *Inorg. Chem.* **2019**, *58*, 603–609. [[CrossRef](#)]
16. Xue, L.; Padgett, C.W.; DesMarteau, D.D.; Pennington, W.T. Synthesis and Structures of Alkali Metal Salts of Bis(Trifluoromethyl)Sulfonyl]Imide. *Solid State Sci.* **2002**, *4*, 1535–1545. [[CrossRef](#)]
17. Nockemann, P.; Thijs, B.; Pittois, S.; Thoen, J.; Glorieux, C.; Van Hecke, K.; Van Meervelt, L.; Kirchner, B.; Binnemans, K. Task-Specific Ionic Liquid for Solubilizing Metal Oxides. *J. Phys. Chem. B* **2006**, *110*, 20978–20992. [[CrossRef](#)]
18. Fujii, K.; Fujimori, T.; Takamuku, T.; Kanzaki, R.; Umebayashi, Y.; Ishiguro, S. Conformational Equilibrium of Bis(Trifluoromethanesulfonyl) Imide Anion of a Room-Temperature Ionic Liquid: Raman Spectroscopic Study and DFT Calculations. *J. Phys. Chem. B* **2006**, *110*, 8179–8183. [[CrossRef](#)]
19. McOwen, D.W.; Seo, D.M.; Borodin, O.; Vatamanu, J.; Boyle, P.D.; Henderson, W.A. Concentrated Electrolytes: Decrypting Electrolyte Properties and Reassessing Al Corrosion Mechanisms. *Energy Environ. Sci.* **2014**, *7*, 416–426. [[CrossRef](#)]
20. Holbrey, J.D.; Reichert, W.M.; Rogers, R.D. Crystal Structures of Imidazolium Bis(Trifluoromethanesulfonyl)Imide 'Ionic Liquid' Salts: The First Organic Salt with a Cis-TFSI Anion Conformation. *Dalton Trans.* **2004**, *15*, 2267–2271. [[CrossRef](#)]
21. Dean, P.M.; Pringle, J.M.; Forsyth, C.M.; Scott, J.L.; MacFarlane, D.R. Interactions in Bisamide Ionic Liquids—Insights from a Hirshfeld Surface Analysis of Their Crystalline States. *New J. Chem.* **2008**, *32*, 2121. [[CrossRef](#)]
22. Mochida, T.; Funasako, Y.; Inagaki, T.; Li, M.-J.; Asahara, K.; Kuwahara, D. Crystal Structures and Phase-Transition Dynamics of Cobaltocenium Salts with Bis(Perfluoroalkylsulfonyl)Amide Anions: Remarkable Odd-Even Effect of the Fluorocarbon Chains in the Anion. *Chem.–Eur. J.* **2013**, *19*, 6257–6264. [[CrossRef](#)] [[PubMed](#)]
23. Traver, J.; Chenard, E.; Zeller, M.; Guillet, G.L.; Lynch, W.E.; Hillesheim, P.C. Directing Cation-Cation Interactions in Thiamine Compounds: Analysis of a Series of Organic Salts Based on Vitamin B1. *J. Mol. Struct.* **2021**, *1232*, 130046. [[CrossRef](#)]

24. Siegel, D.J.; Anderson, G.I.; Cyr, N.; Lambrecht, D.S.; Zeller, M.; Hillesheim, P.C.; Mirjafari, A. Molecular Design Principles of Ionic Liquids with a Sulfonyl Fluoride Moiety. *New J. Chem.* **2021**, *45*, 2443–2452. [[CrossRef](#)]
25. Yoshida, Y.; Saito, G. Ionic Liquids Based on Diethylmethyl(2-Methoxyethyl)Ammonium Cations and Bis(Perfluoroalkanesulfonyl)Amide Anions: Influence of Anion Structure on Liquid Properties. *Phys. Chem. Chem. Phys.* **2011**, *13*, 20302–20310. [[CrossRef](#)] [[PubMed](#)]
26. Henderson, W.A.; McKenna, F.; Khan, M.A.; Brooks, N.R.; Young, V.G.; Frech, R. Glyme–Lithium Bis(Trifluoromethanesulfonyl)Imide and Glyme–Lithium Bis(Perfluoroethanesulfonyl)Imide Phase Behavior and Solvate Structures. *Chem. Mater.* **2005**, *17*, 2284–2289. [[CrossRef](#)]
27. Siraj, N.; Hasan, F.; Das, S.; Kiruri, L.W.; Steege Gall, K.E.; Baker, G.A.; Warner, I.M. Carbazole-Derived Group of Uniform Materials Based on Organic Salts: Solid State Fluorescent Analogues of Ionic Liquids for Potential Applications in Organic-Based Blue Light-Emitting Diodes. *J. Phys. Chem. C* **2014**, *118*, 2312–2320. [[CrossRef](#)]
28. Yim, J.-H.; Oh, B.-K.; Lim, J.S. Solubility Measurement and Correlation of CO₂ in Bis(Pentafluoroethylsulfonyl)Imide ([BETI]) Anion-Based Ionic Liquids: [EMIM][BETI], [BMIM][BETI], [HMIM][BETI]. *J. Chem. Eng. Data* **2020**, *65*, 4378–4386. [[CrossRef](#)]
29. Sun, X.; Luo, H.; Dai, S. Mechanistic Investigation of Solvent Extraction Based on Anion-Functionalized Ionic Liquids for Selective Separation of Rare-Earth Ions. *Dalton Trans.* **2013**, *42*, 8270–8275. [[CrossRef](#)]
30. Tokuda, H.; Hayamizu, K.; Ishii, K.; Susan, A.B.H.; Watanabe, M. Physicochemical Properties and Structures of Room Temperature Ionic Liquids. 1. Variation of Anionic Species. *J. Phys. Chem. B* **2004**, *108*, 16593–16600. [[CrossRef](#)]
31. Siu, B.; Cassity, C.G.; Benchea, A.; Hamby, T.; Hendrich, J.; Strickland, K.J.; Wierzbicki, A.; Sykora, R.E.; Salter, E.A.; O'Brien, R.A.; et al. Thermally Robust: Triarylsulfonium Ionic Liquids Stable in Air for 90 Days at 300 °C. *RSC Adv.* **2017**, *7*, 7623–7630. [[CrossRef](#)]
32. Benchea, A.; Siu, B.; Soltani, M.; McCants, J.H.; Salter, E.A.; Wierzbicki, A.; West, K.N.; Davis, J.H.J. An Evaluation of Anion Suitability for Use in Ionic Liquids with Long-Term, High-Temperature Thermal Stability. *New J. Chem.* **2017**, *41*, 7844–7848. [[CrossRef](#)]
33. Pulido, A.; Chen, L.; Kaczorowski, T.; Holden, D.; Little, M.A.; Chong, S.Y.; Slater, B.J.; McMahon, D.P.; Bonillo, B.; Stackhouse, C.J.; et al. Functional Materials Discovery Using Energy–Structure–Function Maps. *Nature* **2017**, *543*, 657–664. [[CrossRef](#)] [[PubMed](#)]
34. Bruker. *Apex3 V2019.1-0, SAINT V8.40A*; Bruker AXS Inc.: Madison, WI, USA, 2019.
35. Krause, L.; Herbst-Irmer, R.; Sheldrick, G.M.; Stalke, D. Comparison of Silver and Molybdenum Microfocus X-ray Sources for Single-Crystal Structure Determination. *J. Appl. Crystallogr.* **2015**, *48*, 3–10. [[CrossRef](#)] [[PubMed](#)]
36. Bruker. *SHELXTL Suite of Programs, Version 6.14, 2000–2003, Bruker Advanced X-ray Solutions*; Bruker AXS Inc.: Madison, WI, USA, 2000–2003.
37. Sheldrick, G.M. A Short History of SHELX. *Acta Crystallogr. A* **2008**, *64*, 112–122. [[CrossRef](#)]
38. Hübschle, C.B.; Sheldrick, G.M.; Dittrich, B. *ShelXle: A Qt Graphical User Interface for SHELXL*. *J. Appl. Crystallogr.* **2011**, *44*, 1281–1284. [[CrossRef](#)]
39. Dolomanov, O.V.; Bourhis, L.J.; Gildea, R.J.; Howard, J.A.K.; Puschmann, H. OLEX2: A Complete Structure Solution, Refinement and Analysis Program. *J. Appl. Crystallogr.* **2009**, *42*, 339–341. [[CrossRef](#)]
40. Spackman, P.R.; Turner, M.J.; McKinnon, J.J.; Wolff, S.K.; Grimwood, D.J.; Jayatilaka, D.; Spackman, M.A. *CrystalExplorer: A Program for Hirshfeld Surface Analysis, Visualization and Quantitative Analysis of Molecular Crystals*. *J. Appl. Crystallogr.* **2021**, *54*, 1006–1011. [[CrossRef](#)]
41. Spackman, M.A.; McKinnon, J.J. Fingerprinting Intermolecular Interactions in Molecular Crystals. *CrystEngComm* **2002**, *4*, 378–392. [[CrossRef](#)]
42. Spackman, M.A.; McKinnon, J.J.; Jayatilaka, D. Electrostatic Potentials Mapped on Hirshfeld Surfaces Provide Direct Insight into Intermolecular Interactions in Crystals. *CrystEngComm* **2008**, *10*, 377–388. [[CrossRef](#)]
43. Macrae, C.F.; Bruno, I.J.; Chisholm, J.A.; Edgington, P.R.; McCabe, P.; Pidcock, E.; Rodriguez-Monge, L.; Taylor, R.; van de Streek, J.; Wood, P.A. *Mercury CSD 2.0—New Features for the Visualization and Investigation of Crystal Structures*. *J. Appl. Crystallogr.* **2008**, *41*, 466–470. [[CrossRef](#)]
44. Spackman, M.A.; Jayatilaka, D. Hirshfeld Surface Analysis. *CrystEngComm* **2009**, *11*, 19–32. [[CrossRef](#)]
45. McKinnon, J.J.; Spackman, M.A.; Mitchell, A.S. Novel Tools for Visualizing and Exploring Intermolecular Interactions in Molecular Crystals. *Acta Crystallogr. B* **2004**, *60*, 627–668. [[CrossRef](#)] [[PubMed](#)]
46. Rybalova, T.V.; Bagryanskaya, I.Y. C–F ... π , F ... H, and F ... F Intermolecular Interactions and F-Aggregation: Role in Crystal Engineering of Fluoroorganic Compounds. *J. Struct. Chem.* **2009**, *50*, 741–753. [[CrossRef](#)]
47. Arkhipov, D.E.; Lyubeshkin, A.V.; Volodin, A.D.; Korlyukov, A.A. Molecular Structures Polymorphism the Role of F ... F Interactions in Crystal Packing of Fluorinated Tosylates. *Crystals* **2019**, *9*, 242. [[CrossRef](#)]
48. Bauzá, A.; Frontera, A. Electrostatically Enhanced F ... F Interactions through Hydrogen Bonding, Halogen Bonding and Metal Coordination: An Ab Initio Study. *Phys. Chem. Chem. Phys.* **2016**, *18*, 20381–20388. [[CrossRef](#)]
49. Cavallo, G.; Metrangolo, P.; Milani, R.; Pilati, T.; Priimagi, A.; Resnati, G.; Terraneo, G. The Halogen Bond. *Chem. Rev.* **2016**, *116*, 2478–2601. [[CrossRef](#)]
50. Varadwaj, P.; Varadwaj, A.; Marques, H. Halogen Bonding: A Halogen-Centered Noncovalent Interaction Yet to Be Understood. *Inorganics* **2019**, *7*, 40. [[CrossRef](#)]
51. Scheiner, S. F-Halogen Bond: Conditions for Its Existence. *J. Phys. Chem. A* **2020**, *124*, 7290–7299. [[CrossRef](#)]

52. Bernstein, J.; Davis, R.E.; Shimoni, L.; Chang, N.-L. Patterns in Hydrogen Bonding: Functionality and Graph Set Analysis in Crystals. *Angew. Chem. Int. Ed. Engl.* **1995**, *34*, 1555–1573. [[CrossRef](#)]
53. Bissantz, C.; Kuhn, B.; Stahl, M. A Medicinal Chemist's Guide to Molecular Interactions. *J. Med. Chem.* **2010**, *53*, 5061–5084. [[CrossRef](#)]
54. Dunitz, J.D.; Gavezzotti, A. How Molecules Stick Together in Organic Crystals: Weak Intermolecular Interactions. *Chem. Soc. Rev.* **2009**, *38*, 2622. [[CrossRef](#)] [[PubMed](#)]
55. Scilabra, P.; Terraneo, G.; Resnati, G. The Chalcogen Bond in Crystalline Solids: A World Parallel to Halogen Bond. *Acc. Chem. Res.* **2019**, *52*, 1313–1324. [[CrossRef](#)] [[PubMed](#)]